TECHNICAL RESEARCH REPORT

Spectral Filtering for Improved Performance of Collocation Discretization Methods

by Raymond A. Adomaitis

T.R. 2000-6

ISR develops, applies and teaches advanced methodologies of design and analysis to solve complex, hierarchical, heterogeneous and dynamic problems of engineering technology and systems for industry and government.

ISR is a permanent institute of the University of Maryland, within the Glenn L. Martin Institute of Technology/A. James Clark School of Engineering. It is a National Science Foundation Engineering Research Center.

Web site http://www.isr.umd.edu

Spectral Filtering for Improved Performance of Collocation Discretization Methods

Raymond A. Adomaitis
Department of Chemical Engineering and
Institute for Systems Research
University of Maryland, College Park MD 20742
adomaiti@isr.umd.edu

March 9, 2000

Keywords: Orthogonal collocation, spectral filtering, Galerkin method, numerical analysis, Gibbs phenomenon

Abstract

Spectral filtering methods are investigated for use in reducing the Gibbs oscillations that result when discontinuous functions are projected onto globally defined trial function expansions. Several physical-space filters are studied in the context of a high-degree, mixed collocation method used for time integration of a nonlinear boundary value problem with a piece-wise continuous, time-dependent boundary condition. Improved accuracy is reported, both in terms of point-wise and norm-wise solution convergence, making the filtered global collocation approach a potential alternative to spline formulations in some applications.

1 Introduction

Boundary-value problems with spatially discontinuous forcing terms can exhibit poor convergence performance when solutions are represented in terms of a smooth, continuous, globally defined trial function expansion. Likewise, initial conditions that do not satisfy the problem boundary conditions, or discontinuities in the boundary conditions themselves, can result in solutions with non-diminishing oscillations characteristic of the Gibbs phenomenon. In the worst cases, the Gibbs oscillations lead to discretization errors that increase with trial function truncation number, and even in the best cases, give visually unsatisfactory solution profiles. Accurate computation of secondary quantities, such as the flux at a specified spatial location, also can be affected near the discontinuity.

In this paper, we will make use of recent developments in spectral filtering methods as an integral part of discretization procedures based on globally defined trial function solution expansions. We take advantage of computational methods that make possible very high degree discretization levels (Lin, Chang, and Adomaitis, 1999), and use the filtering methods as a means of improving discretization method convergence performance, rather than the more traditional application as a post-processing step. As a representative test case, we consider global polynomial collocation for time integration of a nonlinear boundary-value problem. Collocation-based time integrators have been used in numerous previous applications. Global polynomial collocation methods have been used for optimal control of batch processes (Biegler, 1984) and for solving initial-boundary value problems (Birnbaum and Lapidus, 1978; Villadsen and Sørensen, 1969). Spline collocation methods (collocation on finite elements) have been used extensively for optimal control (Cuthrell and Biegler, 1987, 1998; Logsdon and Biegler, 1993) and parameter estimation (Kim, Liebman, Edgar, 1991) applications, and for the direct computation of limit-cycle solutions (Doedel, 1981). Typically, spline collocation methods are used in place of high-degree global discretization methods and for applications in which discontinuities in time-dependent model parameters are expected. We pose the filtered global collocation approach as an alternative, applicable to some, but certainly not all, situations where a spline collocation method otherwise would be used. The filtered collocation method presented in this paper retains the simplicity of implementation of the traditional global collocation method, simplifying global discretization error analysis and making it attractive for use in process parameter estimation and batch process optimization.

2 The Gibbs phenomenon

To illustrate basic issues in filtering and convergence, consider projecting the piece-wise continuous function defined on the unit interval:

$$f(t) = \begin{cases} 0 & 0 \le t < 0.55 \\ 1 & 0.55 < t \le 1 \end{cases} \tag{1}$$

onto the sequence of trial functions $\psi_{n+1}(t) = P_n(t)/\sqrt{c_n}$ where the shifted Legendre polynomials $P_n(t)$ are defined by the recurrence formula

$$(n+1)P_{n+1}(t) = (2n+1)(2t-1)P_n(t) - nP_{n-1}(t) \tag{2}$$

with $P_0(t) = 1$ and $P_1(t) = 2t - 1$. The resulting sequence of functions is orthogonal with respect to inner product

$$\langle P_m, P_n \rangle = \int_0^1 P_m(t)P_n(t)\,dt = c_n\delta_{m,n}$$

with $c_n = 1/(2n+1)$. Examining the projection $f_N(t)$ of $f(t)$ onto the space spanned by the $\psi_n(t)$, $n = 1, \ldots, N$

$$f_N(t) = \sum_{n=1}^{N} a_n\psi_n(t) \tag{3}$$

with

$$a_n = \langle f(t), \psi_n(t) \rangle,$$

we find the expected Gibbs phenomenon (Fig. 1). Three important features are observed in the projection results. First, oscillatory overshoot behavior near the discontinuity does not vanish with increasing truncation number N, but asymptotically approaches a constant value of approximately 8.949% of the jump magnitude (Gottlieb and Orszag, 1977) as N grows large. Second, the oscillatory effects are exhibited far from the discontinuity: for this problem, pointwise convergence away from the discontinuity and the interval endpoints is of order $1/N$, while at the endpoints convergence is proportional to $1/\sqrt{N}$ (cf. the exponential convergence when $f(t)$ is continuous). The especially poor convergence at the endpoints is directly attributable to the property of the polynomial sequence—that

$$|P_n(t)| < 1, \quad 0 < t < 1$$

but

$$P_n(0) = (-1)^n, \qquad P_n(1) = 1.$$

A third observation comes from comparing consecutive projections f_{N-1} and f_N (Fig. 1). When the ψ_n are taken from an orthogonal sequence, the oscillations tend to become out of phase away from the discontinuity,

and the features near the discontinuity show little change. Therefore, we can average the two consecutive projections in the hope of obtaining better pointwise convergence performance. Continuing this averaging operation on the partial sums extends the smoothing behavior towards the discontinuity (Fig. 1, right). This averaging operation can be expressed by rewriting the partial sum (3) in terms of the spectrally filtered form

$$f_N^\sigma(t) = \sum_{n=1}^{N} a_n \sigma_n \psi_n(t)$$

with the σ_n giving the equivalent to the arithmetic mean of the partial sums f_n, $n = 1, \ldots, N$ (the Cesaro sum):

$$\sigma_n = 1 - \frac{n-1}{N} = 1 - \eta$$

with $\eta = (n-1)/N$. The more uniform, but still slow, pointwise convergence rate is apparent in Fig. 2 (left). In fact, for the representative point chosen for this example, the average partial sum converges at essentially the same rate as the non-filtered projection.

3 Filters

The averaged partial sum filter belongs to the class of first-order filters; a filter of order p is a C^{p-1} function whose first $p-1$ derivatives vanish at $\eta = 0$; specific definitions can be found in Gottlieb and Shu (1997). In the cited reference, it was shown that higher-order filters can provide better point-wise convergence when the filter order grows with truncation number N. One such filter is the Vandeven filter (Vandeven, 1991), derived to produce exponential pointwise convergence of the filtered partial sums away from the discontinuity:

$$\begin{aligned} \sigma(\eta) &= 1 - \frac{(2p-1)!}{(p-1)!^2} \int_0^\eta [s(1-s)]^{p-1}\, ds \\ &= -\frac{(2p-1)!}{(p-1)!^2} \left[\frac{\eta^p}{p} + \sum_{n=1}^{p-1} \frac{(-1)^n (p-1)!}{n!(p-1-n)!} \frac{\eta^{n+p}}{n+p} \right]. \end{aligned}$$

To study the potential improvements in pointwise convergence when using the higher-order filters, we examine $|f_N(t_0) - f_N^\sigma(t_0)|$ as a function of truncation number N and filter order p for the representative point $t_0 = 0.4$. Results are presented in Fig. 2. We observe that convergence for the second-order filter is, in general, better than the other filter orders for $N < 65$. For higher truncation number values, the eighth-order filter gives improved convergence at the point t_0, a result consistent with Gottlieb and Shu (1997).

4 Collocation projection

The tau method (Gottlieb and Orszag, 1977) can be used to force the truncated Legendre polynomial expansion $f_N(t)$ to satisfy a specified set of boundary conditions at $t = 0, 1$. The mixed collocation projection

is the discrete analog to the tau method; while the collocation technique does not necessarily produce results identical to the tau method, the former has the potential of producing better filtered performance because boundary conditions have a more uniform influence on the polynomial mode amplitude values generated by the mixed collocation method.

If the collocation grid points are defined as t_n: $P_{N-2}(t_n) = 0$ plus the interval endpoints, and $\mathbf{f}$ and $\mathbf{a}$ are (column) vectors with elements $f(t_i)$ and a_i (see eqn. 3), $i = 1, \ldots, N$, the discrete transformation array $\mathbf{Q}$

$$\mathbf{f} = \mathbf{Q}\mathbf{a} \tag{4}$$

is defined by

$$Q_{i,j} = \psi_j(t_i).$$

Note that with this definition of $\mathbf{Q}$, instead of the more traditional use of the Vandermonde matrix transpose (Michelsen and Villadsen, 1972; Villadsen and Stewart, 1967), $\mathbf{Q}$ arrays are generated that are numerically nonsingular for $N > 500$. The physical-space filter (defined on the collocation grid) that gives the filtered, discrete-ordinate values $\mathbf{f}^\sigma$ is

$$\begin{aligned} \mathbf{f}_N^\sigma &= \mathbf{Q}\boldsymbol{\Sigma}\mathbf{Q}^{-1}\mathbf{f} \\ &= \mathbf{P_{sp}}\mathbf{f} \end{aligned} \tag{5}$$

with $\Sigma_{i,i} = \sigma_i$ and $\Sigma_{i,j} = 0$, $i \neq j$. The σ_j depend on the filter order; consequently, we denote $\mathbf{P}_{\mathbf{sp}}^{\mathbf{p}}$ as a physical-space filter of order p.

With $\mathbf{f}$ representing (non-filtered) discrete points on (1), the filtered points are computed with (5) and interpolated values are computed using the mode amplitude coefficients obtained from (4). Representative results are presented in Fig. 3. Note that the filtered profiles do not necessarily pass through the original collocation points, but rather through $\mathbf{f}_N^\sigma$. Smoothing by the 2nd-order filter is superior to smoothing by the 8th-order filter near the jump discontinuity due to the overshoot behavior of the higher-order filter. However, at the endpoints, the higher-order filters produce better results.

4.1 Quadrature-based projections – numerical methods

The filtered profiles are reconstructed on a grid finer than the collocation grid to assess the inter-collocation point behavior. Alternatively, we could directly use the interpolation polynomials, but this multiple-grid approach is introduced now because of the computational benefits it will produce when used in computational procedures developed later in this paper. The trial functions are defined on a fine discretization grid $\hat{t}_m$, $m = 1, \ldots, M$ with $M >> N$, in terms of Lagrange interpolation polynomials. The Legendre polynomials are

computed using the recurrence relation (2) on this fine grid. Inner products are computed by quadrature on the fine grid, where the quadrature points $\hat{\mathbf{t}}$ are defined as the combination of the unit interval endpoints and the roots of the Jacobi polynomial $J^{1,1}_{M-2}$, a polynomial sequence orthogonal with respect to inner product weight $t(1-t)$. The projection is reconstructed on the (finer-scale) quadrature grid using

$$\hat{\mathbf{f}}^{\sigma}_{\mathbf{N}} = \hat{\mathbf{\Psi}}\mathbf{Q}^{-1}\mathbf{f}^{\sigma}$$

where $\hat{\Psi}_{i,j} = \psi_j(\hat{t}_i)$. Because we are interested in collocation-based time-integration methods, we also consider the derivative of the filtered function (*not* the filtered derivative) as

$$\frac{d}{dt}\hat{\mathbf{f}}^{\sigma}_{\mathbf{N}} = \hat{\mathbf{\Psi}}\mathbf{Q}^{-1}\mathbf{D}\mathbf{f}^{\sigma}$$

with

$$D_{i,j} = \sum_{k=1}^{N} \frac{d\psi_k(t_i)}{dt} Q^{-1}_{k,j}. \tag{6}$$

We note that the higher-order filters produce less inter-point oscillation near the interval ends, but have an overshoot behavior near the discontinuity that persists in the derivative of the filtered profiles (Fig. 4).

4.2 Modified physical-space filters

The filtered projection convergence behavior at the interval endpoints and near the discontinuity can be explained by examining the physical-space filters themselves (Fig. 5). The second-order filter has an oscillatory behavior that diminishes with increasing distance from the diagonal elements. The oscillations reduce the localizing effect of the filter, allowing the long-range transmission of information from the discontinuity to the interval endpoints and reducing the filter performance near the interval endpoints (Fig. 5, left). The eighth-order filter is much more localized; however, the visible secondary "bumps" lead to the overshoot behavior in the neighborhood of the discontinuity, reducing the filter performance in the neighborhood of the discontinuity but resulting in improved performance near the interval ends.

Because of the drawbacks associated with each of the filters studied, modified physical-space filters were investigated, including those that did not have direct transform-space counterparts. One such filter is generated as a weighted sum of filters of different order. In this composite physical-space filtering approach, two arrays are defined: $\mathbf{P^2_{sp}}$ denoting a second-order physical-space filter and $\mathbf{P^8_{sp}}$ denoting an eighth-order physical-space filter. The composite filter then is computed using

$$\mathbf{P^c_{sp}}_i = 4t_i(1-t_i)\mathbf{P^2_{sp}}_i + (1-4t_i(1-t_i))\mathbf{P^8_{sp}}_i$$

where $\mathbf{P^c_{sp}}_i$ denotes the i-th row of $\mathbf{P^c_{sp}}$. The resulting filter is shown in Fig. 6. We also consider a simple binomial filter, commonly used for image processing applications (Jahne, 1993). It is defined by $P^b_{sp}(i,i) = 1$

for $i = 1, N$ and $P^b_{sp}(i, i-1) = P^b_{sp}(i, i+1) = 1/4$, $P^b_{sp}(i, i) = 1/2$ for $i = 2, \ldots, N-1$; the filter is shown in Fig. 6. Both the composite and binomial filters produced similar results, as measured by the improved convergence near the interval endpoints and the reduced overshoot near the discontinuity. Results for the binomial filter are presented in Figs. 3 and 4.

5 Convergence analysis

To examine the effects filtering has on the convergence of collocation solution procedures, we consider the problem of computing the solution to the boundary-value problem describing the diffusive transport and second-order reaction in a spherical catalyst pellet

$$\frac{\partial C}{\partial t} = \nabla^2 C \ - \phi^2 C^2.$$

This boundary-value problem is subject to boundary conditions

$$\frac{\partial C(0,t)}{\partial r} = 0, \qquad C(1,t) = b(t),$$

initial condition $C(r,0) = b(0)$ for $r < 1$, and the definition of $b(t)$:

$$b(t) = \begin{cases} 0.5 & 0 \le t < t_{max}/2 \\ 1 & t_{max}/2 < t \le t_{max} \end{cases}$$

with $t_{max} = 1$. A semi-discrete Galerkin discretization procedure uses the Q-term trial function expansion to represent the concentration profile in r and t

$$C_Q(r,t) = b(t) + \sum_{q=1}^{Q} a_q(t)\eta_q(r)$$

with the trial functions $\eta_q(r)$ generated from the sequence

$$\left\{ r^{2q-2} \cos(\pi r/2) \right\}_{q=1}^{Q}$$

made orthonormal using the Gram-Schmidt orthogonalization and the weighted inner product

$$\langle \eta_m, \eta_n \rangle_{r^2} = \int_0^1 \eta_m(r)\eta_n(r)\, r^2 \, dr.$$

The Galerkin projection produces the Q nonlinear ordinary equations in time

$$\dot{a}_q(t) = \left\langle -\dot{b}(t) + \nabla^2 C_Q - \phi^2 C_Q^2, \eta_q \right\rangle_{r^2}$$

where the inner product operations are carried out by quadrature on a finer, physical-space discretization grid, similar to the numerical methods discussed in Section 4.1. Writing the mode coefficients $\dot{a}_n$ in (column) vector form gives

$$\dot{\mathbf{a}}(t) = \left\langle -\dot{b}(t) + \nabla^2 C_Q - \phi^2 C_Q^2, \boldsymbol{\eta}^T \right\rangle_{r^2}.$$

We note that written in this way, the projection of the function $C_Q(r,t)$ onto the (column) vector $\boldsymbol{\eta}^T$ produces a column vector. This is important, because if we now expand the vector of equations into the discrete-time form at the t_n, $n = 1, \ldots, N$, we obtain the $Q \times N$ array of equations

$$\dot{\mathbf{A}} = \left\langle -\dot{\mathbf{b}}^T + \nabla^2 \mathbf{C_Q} - \phi^2 \mathbf{C_Q}^2, \boldsymbol{\eta}^T \right\rangle_{r^2}$$

where

$$C_{Q_n}(r) = C_Q(r, t_n) = b(t_n) + \sum_{q=1}^{Q} a_q(t_n)\eta_q(r).$$

The collocation discretization in time gives the large set of nonlinear algebraic equations

$$\mathbf{D}[\mathbf{A}]_2 - \left\langle -(\mathbf{D}\mathbf{b})^T + \nabla^2 \mathbf{C_Q} - \phi^2 \mathbf{C_Q}^2, \boldsymbol{\eta}^T \right\rangle_{r^2} = \mathbf{0} \tag{7}$$

where the notation $\mathbf{D}[\ ]_2$ denotes that the discrete differentiation operation takes place along the second dimension of the array, i.e.,

$$\mathbf{D}[\mathbf{A}]_2 = \mathbf{E}$$

with

$$E_{p,q} = \sum_{k=1}^{N} D_{p,k} A_{q,k} / t_{max}.$$

The fully discretized modeling equation (7) can be solved using the Newton-Raphson method, subject to the concentration initial conditions $a_q(0) = 0$, $q = 1, \ldots, Q$. Representative solution and discretization error results are presented in Fig. 7. The residual function $R(r,t)$ is defined on the quadrature grid as

$$R(\hat{r}_i, \hat{t}_j) = \left[\frac{\partial}{\partial t} - \nabla^2\right] C_Q(\hat{r}_i, \hat{t}_j) + \phi^2 \left[C_Q(\hat{r}_i, \hat{t}_j)\right]^2$$

where the $\hat{r}_i$ and $\hat{t}_j$ are defined by the quadrature grid points (*not* the coarser collocation grid). Standard Lagrange interpolation polynomial collocation is used to define discretized equivalents to both the time and spatial derivatives on the quadrature grid (see Lin, Chang, and Adomaitis, 1999).

5.1 Comparison of filtered and non-filtered methods

When using the non-filtered collocation projection method, the reconstructed $b_N(t)$ shows significant inter-point oscillations, which translate into severe oscillations in $\dot{b}_N(t)$ (Fig. 7). The oscillations affect both the solution and the residual function in the time dimension. When the collocation projection of $b(t)$ is filtered, however, $\dot{b}_N(t)$ is significantly smoother, and the solution is more accurate; the increased accuracy can be seen in the smoother and smaller residual function (Fig. 8). The computational procedure incorporating the composite physical-space filter is nearly identical to the non-filtered technique; however, the problem to be solved now consists of

$$\mathbf{D}[\mathbf{A}]_2 - \left\langle -(\mathbf{D}\boldsymbol{b}^{\boldsymbol{\sigma}})^T + \nabla^2 \mathbf{C_Q} - \phi^2 \mathbf{C_Q}^2, \boldsymbol{\eta}^T \right\rangle_{r^2} = \mathbf{0} \tag{8}$$

with

$$C_Q(r,t_n) = b_n^\sigma + \sum_{q=1}^{Q} a_q(t_n)\eta_q(r)$$

and

$$\boldsymbol{b^\sigma} = \mathbf{P_{sp}^n b}$$

with $\mathbf{n} = \mathbf{2}$, $\mathbf{8}$, $\mathbf{c}$, or $\mathbf{b}$, corresponding to the second, eighth, composite, and binomial filters, respectively. Computing the norm of the fully discretized solution, we find that the filtered solution procedure appears to converge with exponential accuracy, i.e., $\|R(N)\| \approx \alpha \exp(-\beta N)$ for large values of N; furthermore, all of the filtered solutions converge at a comparable rate, a rate substantially better than the non-filtered approach (Fig. 9). A better method for assessing the accuracy of the filtered approaches relative to the non-filtered projection method is to plot the solution residual function norms as a function of the accuracy of the projection of $b(t)$. The accuracy of the filtered projection of $b(t)$ is computed with

$$\|r_b\|^2 = \int_0^{t_{max}} \left[b(t) - b_N^\sigma(t)\right]^2 \, dt$$

and the non-filtered residual is computed analogously. Results presented in Fig. 9 demonstrate that all filtered methods result in substantially increased solution accuracy relative to the non-filtered method when compared on an equal $b(t)$ discretization error basis.

6 Concluding remarks

This paper focused on the application of filtering methods to reduce the Gibbs oscillations that result when discontinuous functions are projected onto globally defined trial function expansions. Various physical-space implementations of the filters were studied and modified to suit the mixed collocation projection method. It was found that a binomial physical-space filter possessed many of the desirable structural attributes of the range of filters examined; the simplicity with which this filter can be generated makes a strong argument for choosing it over the other physical-space filters. With physical-space filter in hand, the convergence of a representative collocation-based discretization application was studied to examine the effect discontinuities had on both normed and point-wise solution convergence. Several methods for quantifying the solution's global accuracy were presented for comparing the filtered and non-filtered approaches. All these methods for assessing solution accuracy demonstrated the substantial improvements produced when filtering was incorporated as part of the collocation solution technique. It was found that the filtered collocation discretization techniques allow high-degree discretizations of problems with time-discontinuous terms that would otherwise make global collocation methods inappropriate.

The original motivation for studying polynomial collocation-based time integration was to expand on the weighted residual methods computational library MWRtools (Adomaitis, Lin, and Chang, 2000; Lin, Chang and Adomaitis, 1999). The goal was to simplify time integration of semi-discretized boundary-value problems, especially those that result in ODE/AE systems. Current work focuses on implementing the polynomial collocation methods in conjunction with developing data structures that define the modeling equations and solution. This work will lead to reducing the bookkeeping involved in simulator development and subsequent modifications. Much of this work is motivated by parameter estimation and batch process optimization applications in chemical vapor deposition reactors and solid-state gas sensor systems model development. Additional details and demonstration scripts can be obtained at the MWRtools project website www.ench.umd.edu/software/MWRtools.

References

[1] Adomaitis, R. A., Y.-h. Lin, and H.-Y. Chang, A computational framework for boundary-value problem based simulations, *Simulation* **74** 30-40 (2000).

[2] Biegler, L. T., Solution of dynamic optimization problems by successive quadratic programming and orthogonal collocation, *Comput. & Chem. Engng* **8** 243-248 (1984).

[3] Birnbaum, I. and L. Lapidus, Studies in approximation methods IV: Double orthogonal collocation with an infinite domain, *Chem. Engng Sci.* **33** 455-462 (1978).

[4] Doedel, E., AUTO: A program for the automatic bifurcation analysis of autonomous systems, *Congressus Numerantium* **30** 265-284 (1981).

[5] Cuthrell, J. E. and L. T. Biegler, On the optimization of differential-algebraic process systems, *AIChE J.* **33** 1257-1270 (1987).

[6] Cuthrell, J. E. and L. T. Biegler, Simultaneous optimization and solution methods for batch reactor control profiles, *Comput. & Chem. Engng* **13** 49-62 (1988).

[7] Gottlieb, D. and S. A. Orszag, *Numerical Analysis of Spectral Methods* SIAM CBMS-NSF Regional Conf. Series in Appl. Math. Vol. 26, 1977.

[8] Gottlieb, D. and C. -W. Shu, On the Gibbs phenomenon and its resolution, *SIAM Rev.* **39** 644-668 (1997).

[9] Jahne, B., *Digital Image Processing. Concepts, Algorithms, and Scientific Applications, 2nd Ed.*, Springer-Verlag, Berlin (1993)

[10] Kim, I.-W, M. J. Liebman, and T. F. Edgar, A sequential error-in-variables method for nonlinear dynamic systems, *Comput. & Chem. Engng* **15** 663-670 (1991).

[11] Lin, Y. -h., Chang, H. -Y., and R. A. Adomaitis, MWRtools: A library for weighted residual methods, *Computers & Chem. Engng* **23** 1041-1061 (1999).

[12] Logsdon, J. S. and L. T. Biegler, A relaxed reduced space SQP strategy for dynamic optimization problems, *Comput. & Chem. Engng* **17** 367-373 (1993).

[13] Michelsen, M. L. and J. Villadsen, A convenient computational procedure for collocation constants, *Chem. Engng L.* **4** 64-68 (1972).

[14] Vandeven, H., Family of spectral filters for discontinuous problems, J. Sci. Comput. **6** 159-192 (1991).

[15] Villadsen, J. and J. P. Sørensen, Solution of partial differential equations by a double collocation method, *Chem. Engng Sci.* **24** 1337-1349 (1969).

[16] Villadsen, J. V. and W. E. Stewart, Solution of boundary-value problems by orthogonal collocation. *Chem. Engng Sci.* **22** 1483-1501 (1967).

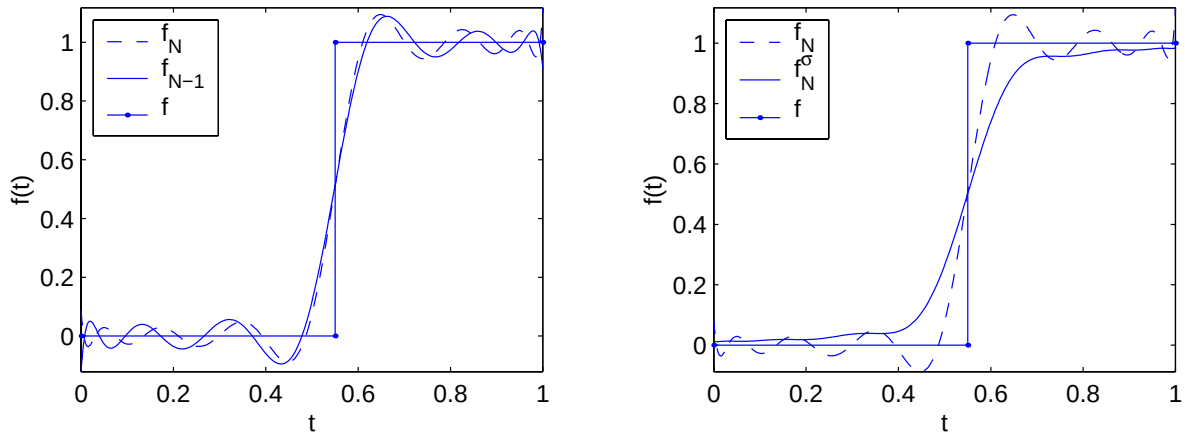

Figure 1: *Gibbs oscillations in two consecutive projections (left) for* $N = 15$*; First-order filtered results (right).*

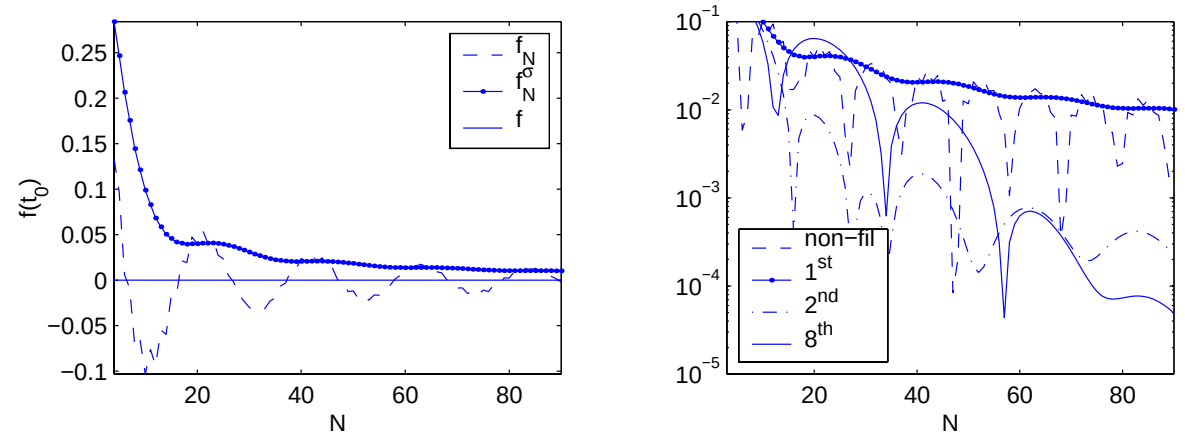

Figure 2: *Pointwise convergence of* $f_N(t_0)$ *and* $f_N^\sigma(t_0)$ *at* $t_0 = 0.4$ *for non-filtered and 1st-order filtered projections (left). Convergence of* $|f_N(t_0) - f_N^\sigma(t_0)|$ *for* $t_0 = 0.4$ *(right), comparing non-filtered results to those obtained using three different filter orders.*

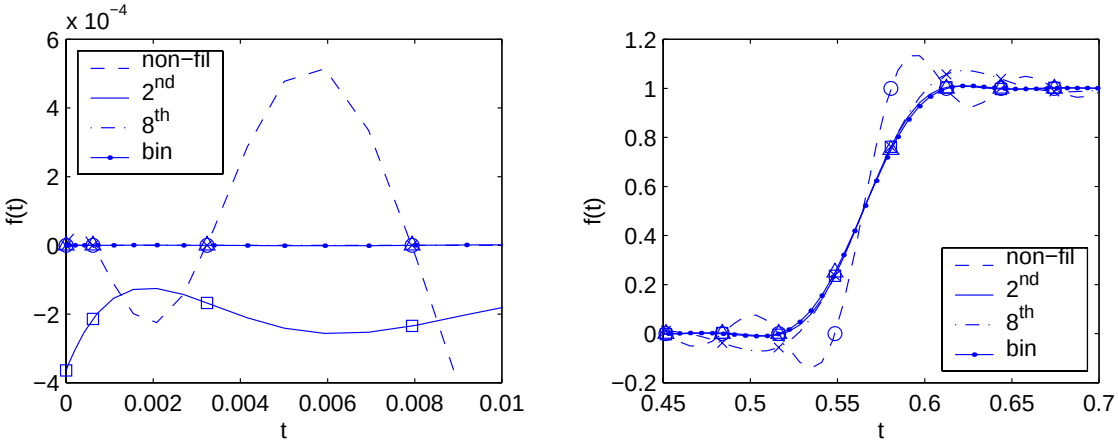

Figure 3: *Collocation projection results; non-filtered results compared to several physical-space filters away (left) and near (right) the discontinuity. Note that the binomial and eighth-order filters produce nearly identical results near the interval ends. Collocation points for the non-filtered, 2nd, 8th, and binomial filtered projections are marked by* ∘, □, ×, *and* △, *respectively.*

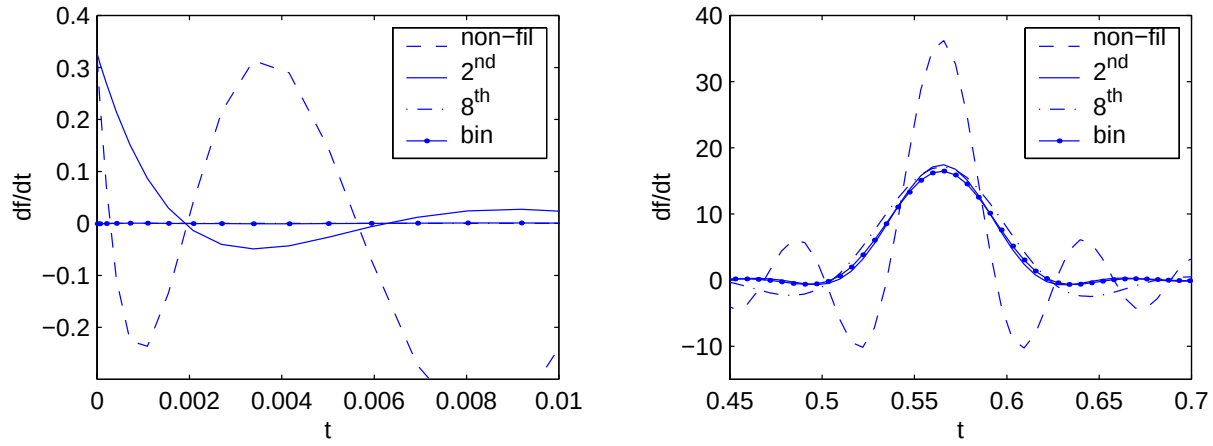

Figure 4: *Oscillations in the first derivative of non-filtered and filtered collocation projections. Again, the binomial and eighth-order filters produce nearly identical results near the interval ends.*

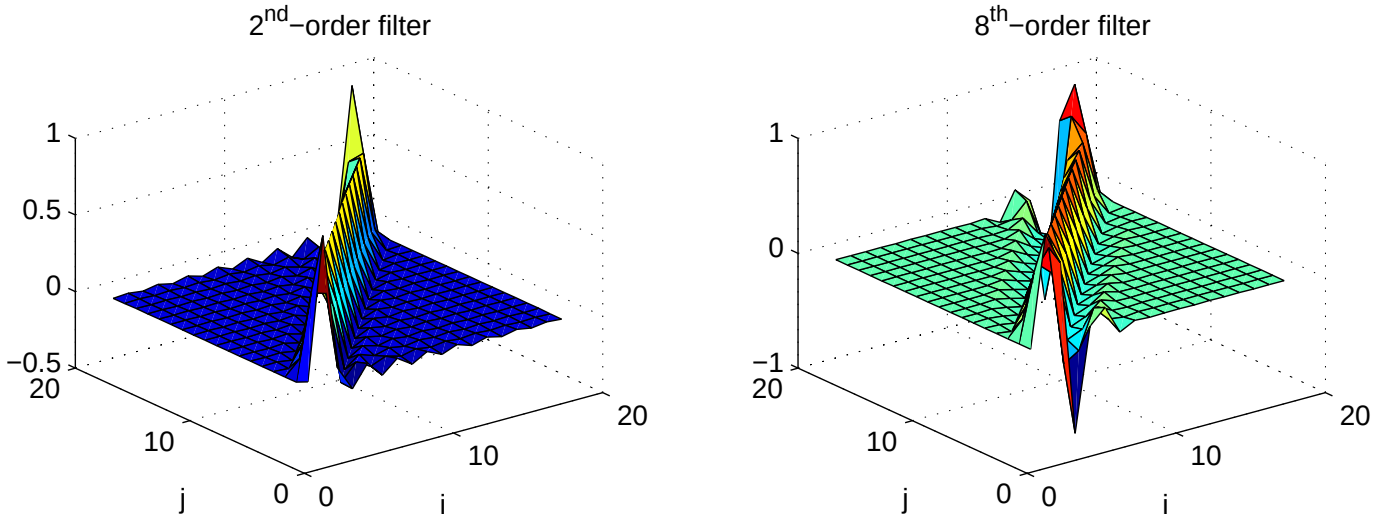

Figure 5: *The physical-space filters corresponding to the Vandeven filter with* $N = 18$.

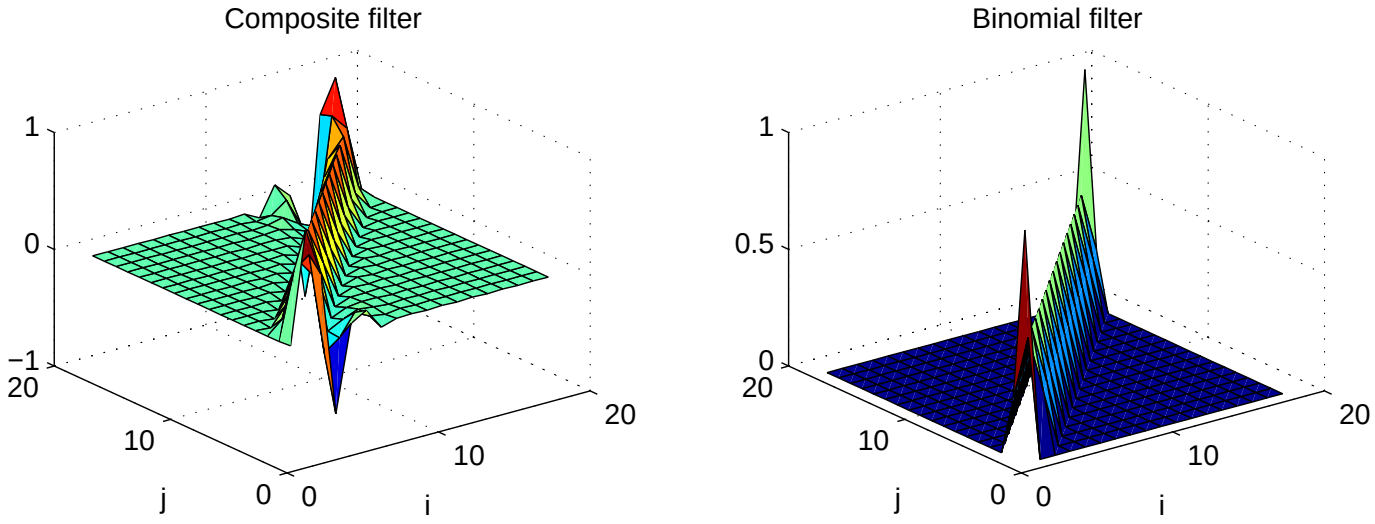

Figure 6: *Composite and binomial physical-space filters for* $N = 18$.

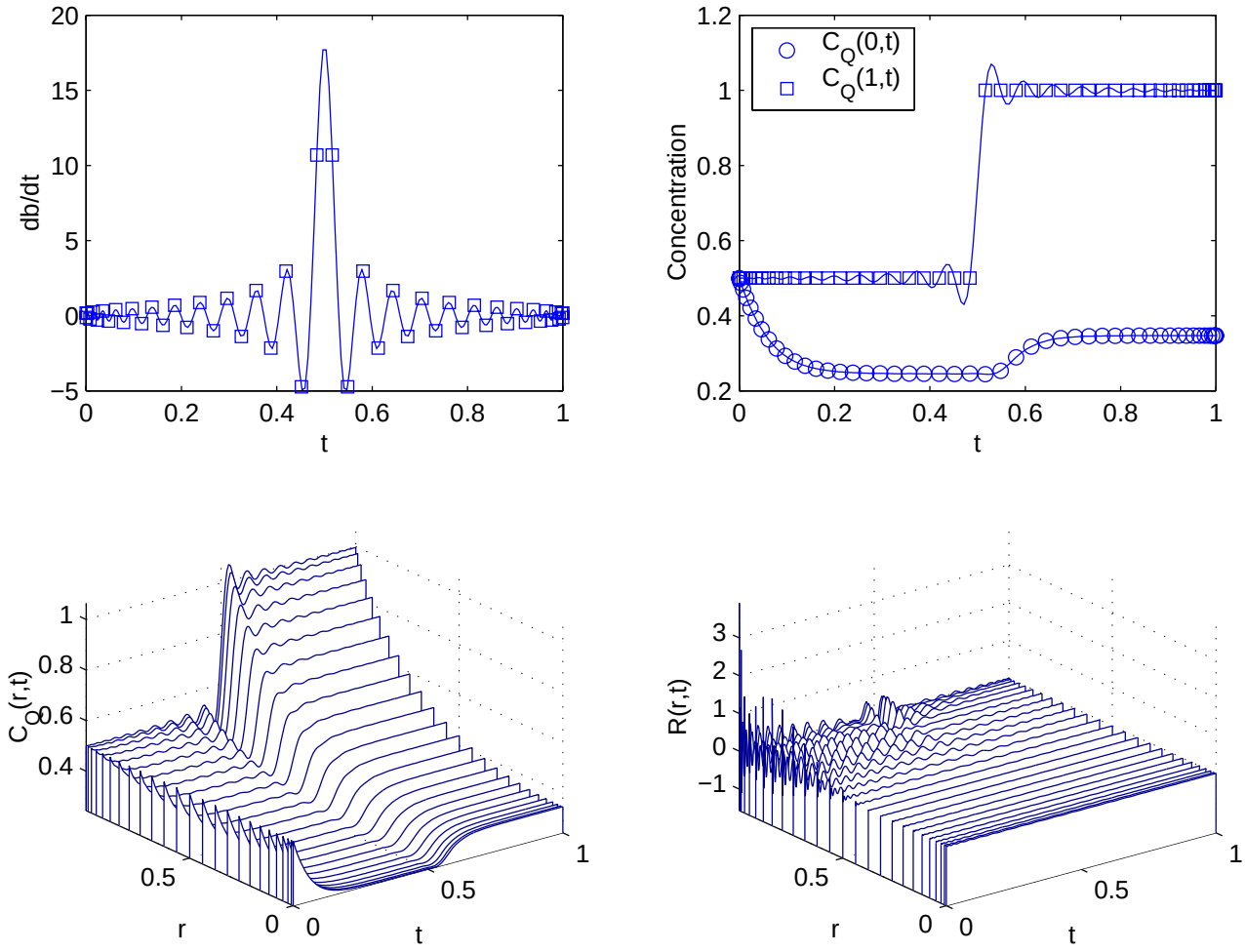

Figure 7: *Simulation results produced using* $N = 50$, $Q = 10$, *and* $\phi = 4$, *based on using an non-filtered* $b(t)$. *Shown are the forcing function time derivative (top left), reactant concentration at* $r = 0, 1$ *(top right), the concentration profile (bottom left), and the residual function (bottom right).*

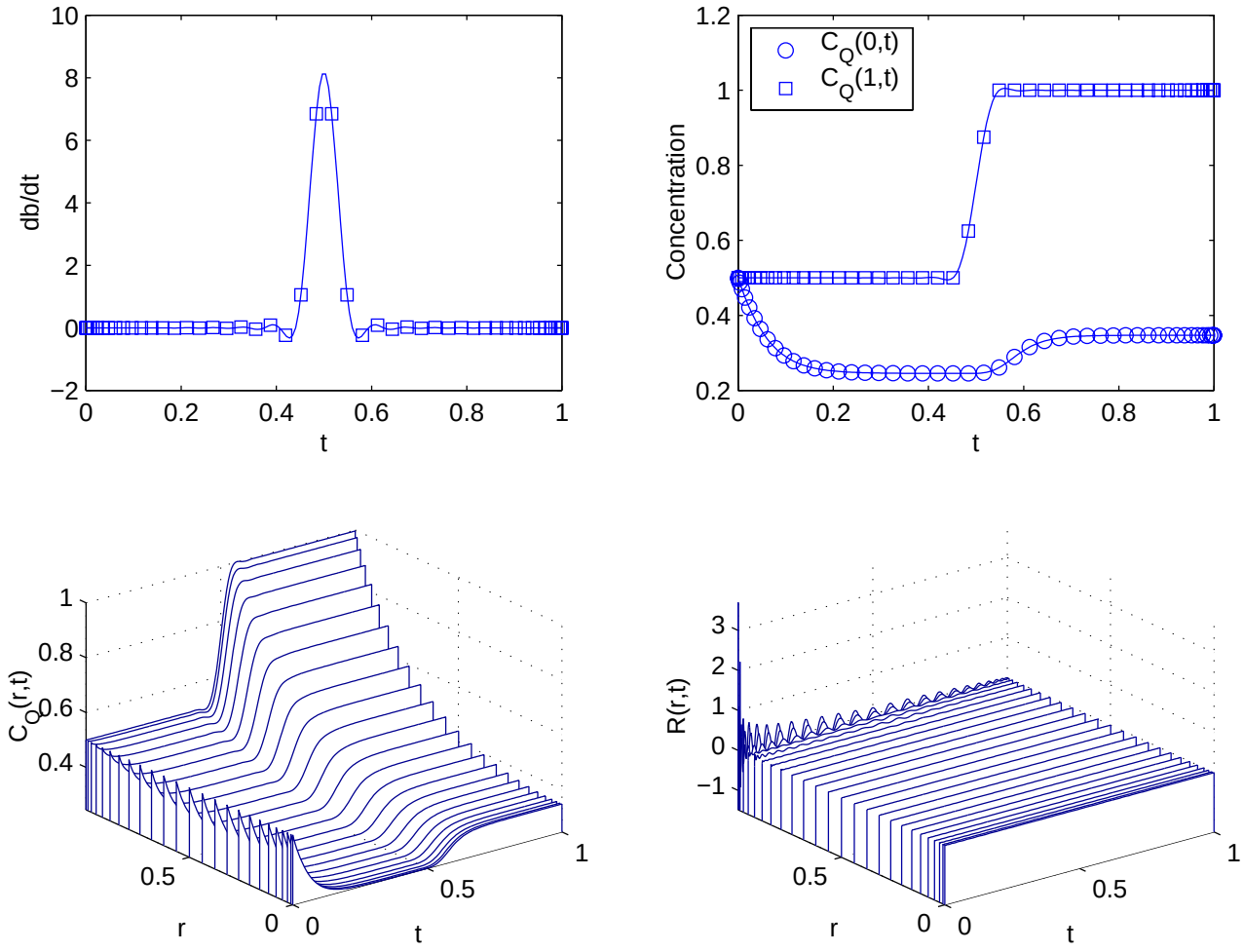

Figure 8: *Simulation results produced using* $N = 50$, $Q = 10$, *and* $\phi = 4$, *based on using a (binomial) filtered* $b(t)$. *Figure format is the same as Fig. 7.*

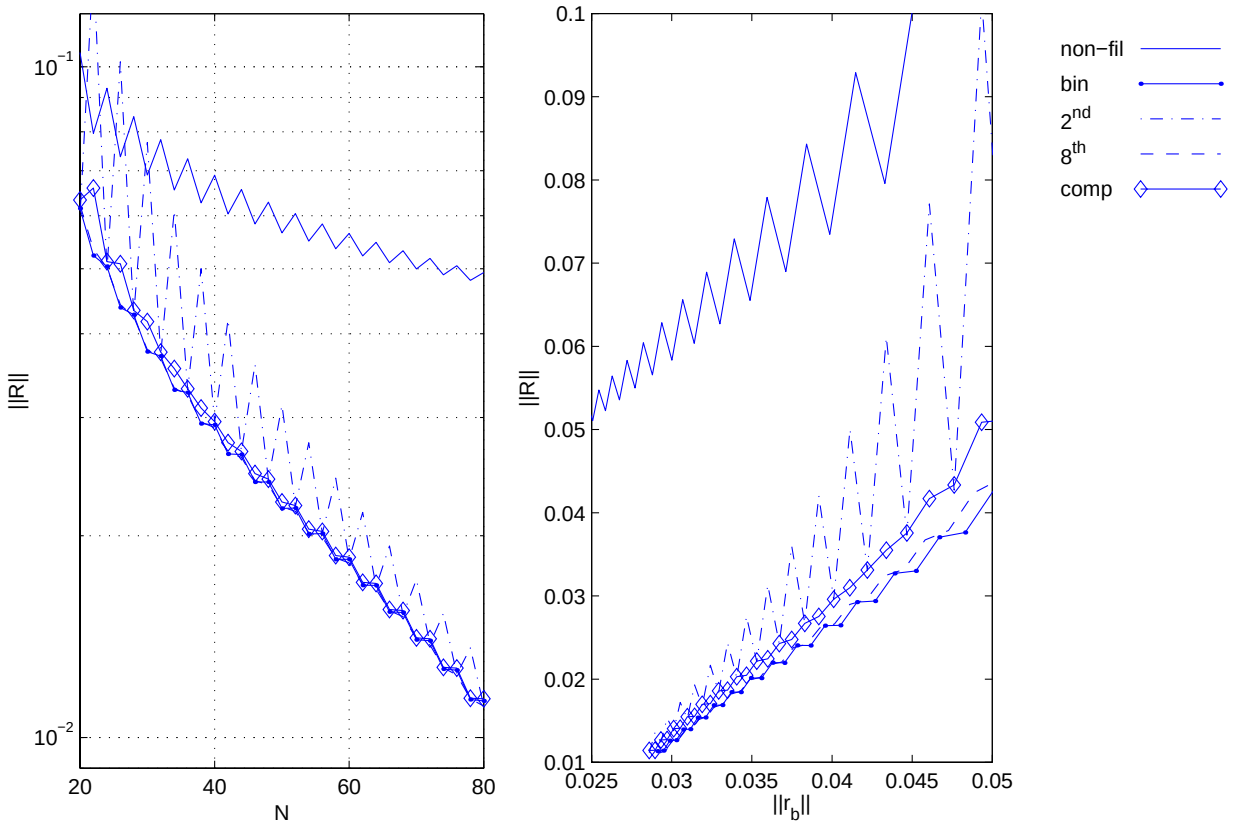

Figure 9: *Residual norm of the fully discretized solution plotted as a function of collocation number (left) and as a function of $b(t)$ projection residual norm (right). Note that the curves representing the 8^{th} order, binomial, and composite filters fall nearly on top of each other.*